


## Hubble speed from first principles

Fabrizio Renzi\* and Alessandra Silvestri

*Lorentz Institute for Theoretical Physics, Leiden University, P.O. Box 9506, Leiden 2300 RA, Netherlands*

 (Received 26 May 2021; revised 25 September 2021; accepted 19 December 2022; published 19 January 2023)

We introduce a way of measuring  $H_0$  from a combination of independent geometrical data sets, without the need for calibration or the choice of a cosmological model. We build on the distance duality relation, which sets the ratio of the luminosity and angular diameter distance to a fixed scaling in redshift for any metric theory of gravity with standard photon propagation and constitutes a founding block of any theory describing our Universe. Our method allows us to determine  $H_0$  from first principles, unleashing the measurement of this fundamental constant from calibration and the assumption of a cosmological model. We find  $H_0 = 69.5 \pm 1.7$  km/s/Mpc at 68% C.L., showing that the Hubble constant can be constrained at the percent level with minimal assumptions.

DOI: [10.1103/PhysRevD.107.023520](https://doi.org/10.1103/PhysRevD.107.023520)

### I. INTRODUCTION

The Hubble parameter  $H_0$  is arguably the most fundamental constant of our Universe. This parameter provides its current expansion rate, an indication of its age, and an overall scale for distances. After almost a century of increasingly precise determinations [1], two leading experiments now report values of  $H_0$  in tension at more than  $4\sigma$ :  $H_0 = 74.03 \pm 1.42$  km/s/Mpc at 68% C.L. from Type Ia supernovae (SNIa) calibrated using Cepheid variable stars from the SH0ES Collaboration [2]<sup>1</sup> and  $H_0 = 67.4 \pm 0.5$  km/s/Mpc 68% C.L. inferred by Planck from the cosmic microwave background (CMB), within the standard cosmological model  $\Lambda$ CDM [5]. Some yet unaccounted for systematics in CMB [5–9] or SNIa [10–14] data or a modification of the standard cosmological model (for recent reviews, see, e.g., Refs. [15,16]) could reconcile these measurements; however, no compelling resolution in either direction has been found yet.

A recent reanalysis of the Planck data [17] has shown that the results on cosmological parameters inferred from the Planck likelihood show no evidence of being affected by any significant systematic error. In addition, results from recent CMB ground experiments

have obtained results consistent with Planck, within  $\Lambda$ CDM [18–21].<sup>2</sup> The SH0ES team has also performed an extensive analysis of possible systematic errors in the SNIa calibration procedure and Cepheid measurements, as well as their impact on the determination of  $H_0$  [2–4], excluding a full resolution of the tension with Planck via a systematic error. The SH0ES Collaboration used the light curves of variable Cepheid stars to anchor SNIa and infer  $H_0$ . While these methods are robust, some unaccounted-for systematics could be causing the SH0ES value to be in tension with Planck [12]. Different methods of calibration, using either the surface brightness fluctuations of SNIa (SBF) or the tip of the red giant branch (TRGB), have, respectively, measured a value of  $H_0 = 70.50 \pm 5.75$  km/s/Mpc [22] and  $H_0 = 69.6 \pm 1.9$  km/s/Mpc [23]. This discrepancy traces back to a difference in the inferred absolute magnitude of SNIa and results in an inconsistency at  $2\sigma$  in their measure of distances to common SNIa hosts [12].

The expansion rate of the universe sets the scaling of distances with time. In such a universe, described by the Friedmann-Lemaître-Robertson-Walker (FLRW) metric,  $ds^2 = -dt^2 + a^2(t)d\chi^2$  (where we set  $c = 1$ ), the comoving distance  $\chi$  is related to the evolution of the scale factor  $a(t)$  via

$$\frac{d\chi}{dz} = H^{-1}(z), \quad (1)$$

where we have introduced the redshift  $z$  via the relation  $a = (1+z)^{-1}$ , and  $H(z)$  is the Hubble parameter, i.e., the

\*renzi@lorentz.leidenuniv.nl

<sup>1</sup>This result has recently been updated by the SH0ES Collaboration with the new parallax measurements of nearby Cepheids from the GAIA satellite [3]. The new constraint on the Hubble constant slightly improved in accuracy, leading to  $H_0 = 73.30 \pm 1.04$  km/s/Mpc. However, the improved data have not yet been made public; therefore, we continue to refer to the results presented in [4] in order to allow for a more informed comparison of our results. Comparing our findings with the latest SH0ES result would lead to raising the statistical significance of the discrepancy with our  $H_0$  to around  $0.5\sigma$ .

<sup>2</sup>It is worth noting that those experiments employed prior information on the cosmic optical depth coming directly from Planck. Therefore, they cannot be considered completely independent from the Planck measurements.

rate at which the universe is expanding at a given time  $H(t) \equiv d \ln a / dt$  expressed in terms of  $z$ , with  $H(z=0) = H_0$  today.

The evolution of the Hubble parameter depends on the cosmological model, and to highlight this we write

$$\chi(z) = \frac{1}{H_0} \int_0^z \frac{d\tilde{z}}{E(\tilde{z})}, \quad (2)$$

where

$$E^2(z) \equiv \frac{H^2(z)}{H_0^2} = \Omega_m(1+z)^3 + \Omega_r(1+z)^4 + \Omega_X X(z). \quad (3)$$

With  $\Omega_X$  we broadly indicate any contribution to  $H(z)$  not coming from matter or radiation; e.g.,  $\Lambda$ CDM with nonzero spatial curvature would give  $\Omega_X \neq 0$ . The possible time dependence of any kind of dynamical dark energy or modification of gravity will be captured by  $X(z)$ , with  $X = 1$  corresponding to the cosmological constant  $\Lambda$  [24].

These equations show that by reconstructing the evolution of cosmic distances in redshift, we can probe not only into the dynamics of the universe but also into its composition or, more broadly, its cosmological model  $E(z)$ . They also highlight how the inference of cosmological parameters from distances is inevitably characterized by a strong correlation between  $H_0$  and the cosmological model, which is more severe at higher redshift. This is why the so-called early-time measurements of  $H_0$ , e.g., CMB, are model dependent. Low redshift, late-time measurements such as SNIa probe  $H_0$  more directly, as can be seen from the  $z \rightarrow 0$  limit of Eq. (2); yet they crucially depend on an overall calibration of nearby distances. To shed light on the Hubble tension, we seek a way to constrain  $H_0$  independently of any assumption on the cosmological model and calibration.

## II. FROM DISTANCES TO THE HUBBLE PARAMETER

Cosmological observations measure the flux from sources of known intrinsic brightness (inferring the luminosity distance  $d_L$ ) or the angular scale of an object of known size (inferring the angular diameter distance  $d_A$ ). They are both related to the comoving distance, albeit in a model-dependent way. On more general terms, in any metric theory of gravity, if photons propagate along null geodesics and obey number conservation, it is possible to show that at any redshift

$$\eta(z) \equiv \frac{d_L(z)}{(1+z)^2 d_A(z)} = 1, \quad (4)$$

based solely on general geometrical arguments [25]. Equation (4) is known as the distance duality relation (DDR). We focus, quite generally, on theories for which the

DDR holds, which means frameworks with a metric theory of gravity and standard photon propagation. Hence,  $\eta$  is set to unity by the theory. On a side note, we see that experimental constraints have been placed on  $\eta$ , which allow only tiny deviations from unity at the order of  $10^{-2}$ – $10^{-1}$  [26–31]. While the DDR is independent of the choice of the metric and is based solely on metricity and standard photon propagation, in what follows we still adopt a FLRW metric, both when connecting observable quantities to cosmological distances and in the values of some data parameters (such as the magnitude intercept in SHOES).

Setting  $\eta = 1$ , Eq. (4) can then be rewritten as

$$H_0 = \frac{1}{(1+z)^2} \frac{H_0 d_L(z)}{H(z) d_A(z)} H(z). \quad (5)$$

The term in the denominator,  $H(z) d_A(z)$ , can be obtained from a combination of line-of-sight and transverse BAO measurements, without the need for an external anchor for the sound horizon  $r_s$  at the drag epoch (as we will discuss in more detail in Sec. III). Cosmic chronometers (CC) are standard clocks which, combining differential age estimates of systems with passively evolving star populations (e.g., very massive and passively evolving galaxies) with their corresponding spectroscopic redshift, determine  $H(z) = -(1+z)^{-1} \Delta z / \Delta t$ . As such, they provide  $H(z)$  data that are free from calibration and do not depend on the underlying cosmological model [32–36]. As we discuss in Appendix B, they carry some dependence on astrophysical modeling. Finally,  $H_0 d_L$  can be obtained from measurements of SNIa without the need for calibration. Combining BAO and CC first, and then folding in SNIa, we obtain

$$H_0 = \frac{1}{(1+z)^2} \frac{[H_0 d_L(z)]^{\text{SNIa}}}{[d_A(z)]^{\text{BAO+CC}}}. \quad (6)$$

We get  $[H_0 d_L(z)]^{\text{SNIa}}$  directly from the measurements of apparent magnitude through  $m_B = 5 \log_{10}(H_0 d_L) - 5a_B$  (where we fix  $a_B = 0.71273 \pm 0.00176$  as inferred in [4] directly from the same SNIa measurements that we are using, and independently of CMB and BAO). The values of  $m_B$  we used in this work are the standardized apparent peak magnitude of SNIa as listed in the Pantheon catalog. This is a heavily processed quantity derived from analyzing the light curves of each SNIa in the catalog. The Pantheon catalog contains thousands of such measurements collected from different experiments and reanalyzed to smooth over the peculiar features of each survey (for more details about the SNIa standardization process, we refer to [37] and references therein). It is worth noting that using this value of  $a_B$  bears some minimal model dependence in the choice of the form of the expansion rate. Such assumptions have been reviewed in the latest SHOES release [3], showing no sign of inconsistency with the assumptions made in [4].

Using the combination in Eq. (6), we can then estimate  $H_0$  without relying on the choice of a cosmological model.

However, assuming the validity of the DDR is equivalent to assuming that all probes are consistent tracers of the cosmic expansion. If this was not the case, the  $H_0$  inferred from Eq. (6) would not be a constant, but rather it would show some trend in redshift. The reformulation of the DDR in terms of Eq. (6) makes manifest the role of  $H_0$  not only as an absolute distance scale but also as a trigger of inconsistencies among distance probes. In particular, an inconsistency in  $H_0$  from two experiments probing the same redshift necessarily corresponds to an inconsistency in their distances. This is the case, for example, for the  $2\sigma$  discrepancy between the value of  $H_0$  from TRGB and SH0ES, which can be linked to an inconsistency at  $2\sigma$  in their measures of distances to common SNIa hosts [12]. Other minimally model-dependent methods to estimate  $H_0$  have been proposed in the literature in recent years: for example, methods that employ interpolation of the expansion history  $H(z)$  and extrapolate towards  $H_0$  [38–42] or employ the inverse distance ladder [43–46]. Typically, these methods still carry some dependence on the value of the drag scale  $r_s$  [41,46] and/or other cosmological parameters (e.g., curvature density [38–40,42–45]). With our approach, we further remove such dependence and effectively only rely on the assumption of the validity of the DDR.

### III. DATA SETS AND METHODOLOGY

We use three publicly available data sets: the Pantheon data set [37], a collection of around 1000 SNIa relative brightness measurements; seven BAO data points from the last data release of the BOSS Collaboration (see Table II); and a compilation of 30 CC measurements of  $H(z)$  in the interval  $0 < z < 2$  [32–36] (see Table I).

These data sets cover almost the same range of redshift ( $0 < z \lesssim 2$ ); therefore, they measure the very same volume of the universe with three independent methods. Yet, they are discrete and provide measurements of  $H(z)d_A(z)$ ,  $H_0d_L(z)$ , and  $H(z)$  at different redshifts. We choose to work with the seven redshift points corresponding to the BAO data set and apply a Gaussian process (GP) regression to fit to SNIa and CC in order to reconstruct them at the chosen redshifts. At each redshift, the GP regression estimates the expected value of the reconstructed function and its confidence interval, providing us with a continuous set of probability distribution functions (PDFs) at any given redshift. The outcome of this procedure is therefore a multidimensional probability distribution in the functional space of  $H_0d_L(z)$  and  $H(z)$ , predicting the behavior of these functions where data are not available. In Fig. 1 we show the outcome of the GP fits to the  $H(z)$  data from CC and to the (binned) magnitude data of SNIa, with different kernels shown in different colors. One can clearly notice that all kernels give a very good representation of the

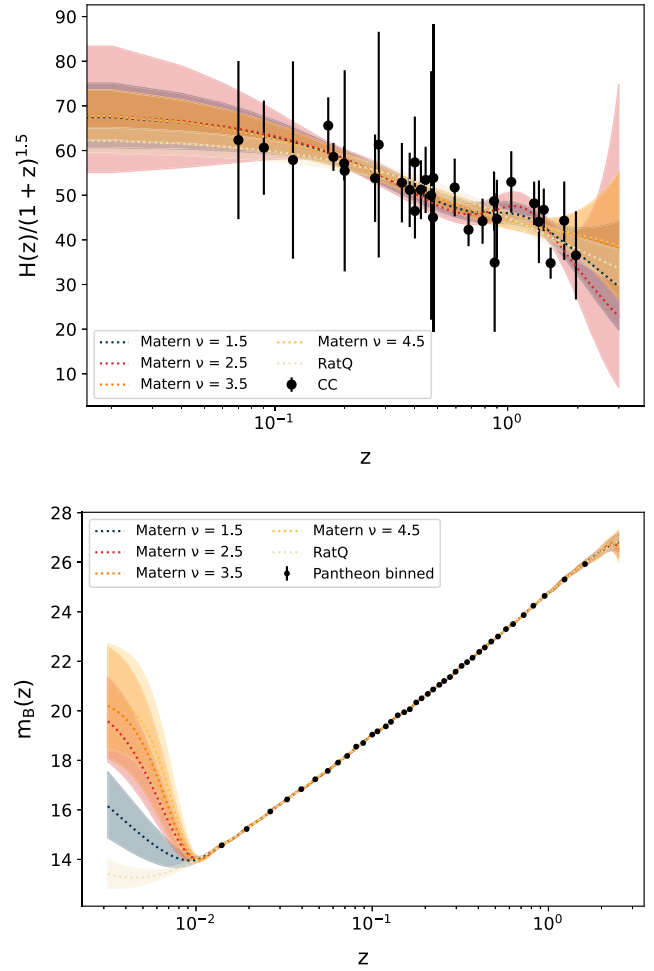


FIG. 1. GP interpolations of the CCH (upper panel) and SNIa (bottom panel) data with different kernels from the Matern family [Eq. (A3)] as well as with the RatQ kernel [Eq. (A2)]. The fits are shown against the data (black dots), which in the SNIa case are the binned Pantheon data. Different colors correspond to different kernels, as shown in the legend. For each kernel, the solid line represents the mean, and the three corresponding shaded regions represent the  $1\sigma$  level.

measurements in the range where data exist, with negligible differences among the different kernels. However, outside the data range, the fit becomes unreliable, with, in some cases, severe differences among the different kernels, highlighting the biasing potentially introduced by extrapolations. In our analysis we rely on the GP fit strictly within the redshift range of data. In the latter, we choose the representation of the GP that gives the lowest  $\chi^2$ , i.e., the rational quadratic (RatQ) for the CCH measurements and the Matern kernel for the SNIa data with shape parameters  $\nu = 2.5$  (see Appendix A for more details on the  $\chi^2$  calculation and on the form of kernels).

The resulting GP fit to the luminosity distance of SNIa is shown in the bottom panel of Fig. 2, against the Pantheon data and the  $\Lambda$ CDM prediction.

From these fits, we extract random variate (samples) of the PDF of  $H_0 d_L(z)$  and  $H(z)$  at the BAO redshifts. In other words, we extract a number of realizations compatible with the statistics dictated by the distribution function of the GP fit. Specifically, we draw  $10^4$  realizations of  $H_0 d_L(z)$  and  $10^4$  realizations of the expansion rate  $H(z)$ . As for the BAO data, we do not perform any GP fit, and we use their seven redshift points as the reference ones. We combine the BAO data in Table II, i.e.,  $d_M/r_s$  and  $d_H/r_s$ , assuming they have Gaussian PDFs (based on the symmetry of their 68% confidence intervals), to obtain PDFs of  $H(z)d_A(z)$  at the seven redshifts.

We proceed by combining the realizations of CC  $H(z)$  (from the GP fit) with the unanchored BAO data  $H(z)d_A(z)$  to obtain  $10^4$  samples of the angular distance  $[d_A(z)]^{\text{BAO+CC}}$  at the seven BAO redshifts. We show the corresponding estimates in the upper panel of Fig. 2 (orange dots), along with the  $\Lambda\text{CDM}$  prediction for  $d_A(z)$  and a simple GP fit to  $[d_A(z)]^{\text{BAO+CC}}$ . We do not use this latter fit in the subsequent steps, but it still provides a useful check for any deviations with respect to the standard cosmological model in our reconstruction of the BAO distance. This procedure of calibrating BAO from the CC data directly provides estimates of the value of  $d_A(z)$  at several redshifts, without any dependence on the cosmological model or on the physics of recombination.

It is certainly true that by combining the  $d_M$  and  $d_H$  data, one effectively reduces the constraining power of BAO; however, one gains independence from calibrations of the sound horizon or assumptions on the cosmological model. Any other way of using the BAO data to infer  $H_0$  would include one or more of the latter. For instance, one could calibrate the BAO directly using the CC measurements as done, e.g., in [39,40], but this requires one to make an assumption about the form of the expansion history and to include the curvature density in the analysis. Another possibility would be to constrain the combination  $r_s H_0$  (which can be fixed without including high redshift information and the curvature density [41]); however, this would not provide a measure of the Hubble constant independent of the value of the sound horizon. Finally, as proposed in [57,58], it is possible to combine BAO data and big bang nucleosynthesis (BBN) to estimate the sound horizon  $r_s$ . However, BBN codes depend on the knowledge of the value of the neutron lifetime, which is used to calculate the abundance of primordial elements. Currently there is a  $4\sigma$  discrepancy in the measurements of the neutron lifetime between bottle-only and beam-only experiments (see, e.g., Refs. [59,60]). A change in the neutron lifetime can significantly bias the constraints from BAO data (particularly the value of  $N_{\text{eff}}$  [61]) and lead to a biased  $H_0$  inference.

We proceed by combining  $10^4$  realizations of the uncalibrated  $[H_0 d_L(z)]^{\text{SNIa}}$  with an equal number of realizations of  $[d_A(z)]^{\text{BAO+CC}}$  by means of Eq. (6) to get an

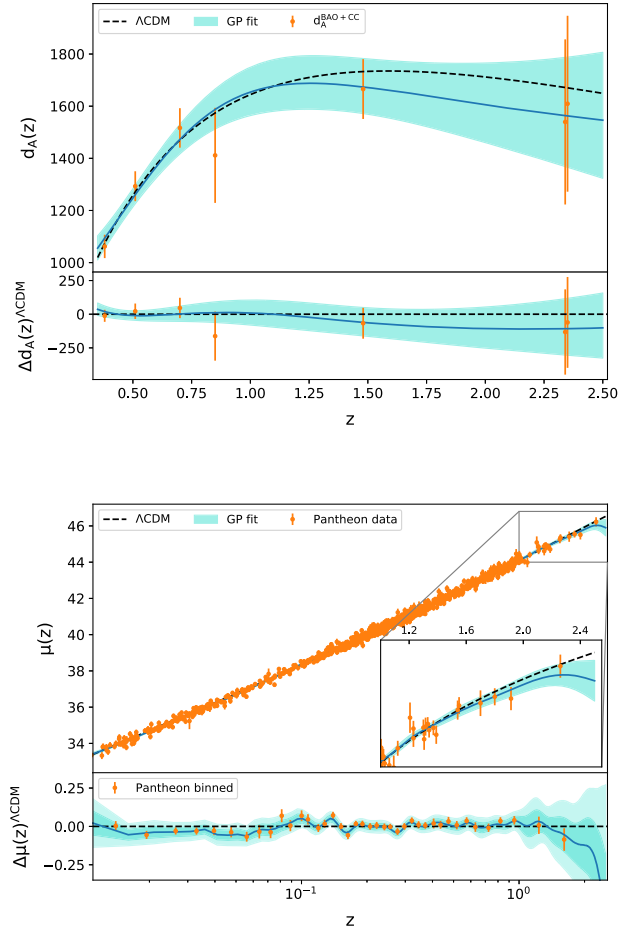


FIG. 2. Top panel: angular diameter distance reconstructed from BAO and CC data, and corresponding residual. The points with error bars correspond to the data reconstructed via the GMC applied to the BAO and CC measurements; the solid blue curve is the GP fit to the data points. Bottom panel: GP fit to the luminosity distance from SNIa (Pantheon) data. In both panels, the dashed black curve shows the  $\Lambda\text{CDM}$  model predictions corresponding to our best-fit  $H_0$  and  $\Omega_m = 0.3$ , with respect to which the residuals are calculated.

estimate of the PDF of  $H_0$  at each of the BAO redshifts (Fig. 3).

With the above procedure, the uncertainty on  $[H_0 d_L]^{\text{SNIa}}(z)$  and  $[d_A]^{\text{BAO+CC}}(z)$ , as well as their mutual correlation, is intrinsically included in the respective PDFs. We base our error propagation on the PDF samples (see also [62]) to take advantage of this feature. For every sample of the PDFs of  $[H_0 d_L]^{\text{SNIa}}(z)$  and  $[d_A]^{\text{BAO+CC}}(z)$ , we calculate the corresponding sample of the posterior of  $H_0$  through Eq. (5). We then use these samples to reconstruct the multidimensional distribution of the seven  $H_0$  measurements. This is analogous to the procedure used in MCMC to derive constraints on the likelihood parameters and allows one to translate the correlations and the uncertainties of the PDFs of the distances directly into the PDFs of  $H_0$ . This guarantees that the correlations between

individual  $H_0$  and their errors are accounted for, and it further allows us not to make any specific assumption about the form of the PDFs of  $H_0$  (e.g., approximating them to Gaussian PDFs). From the latter, we extract the *marginal* distribution of the individual  $H_0$ , thus leaving us with seven uncorrelated PDFs. Finally, we multiply together all the marginalized PDFs of  $H_0$  into a single PDF from which one can easily extrapolate the mean and variance by employing an inverse transform sampling. This is done by assuming a uniform prior range for  $H_0$  and then calculating the product of the probability of each of the seven marginalized  $H_0$  PDFs. The latter, as well as the PDF resulting from multiplying them, are reported in Fig. 3. We discuss the impact of choosing the likelihood constructed with the marginalized PDFs in Appendix C.

The overall method is a combination of a MCMC-like parameter estimation and a Gaussian process reconstruction, and we refer to it as Gaussian process Monte Carlo (GPMC). It uses the least possible number of theoretical assumptions to derive cosmological information and provide results that

are conditioned only by the GPMC reconstruction. We purposely avoid any external calibration of our data set or assumption on the cosmological model. We also choose not to extrapolate the GP fit to  $z \rightarrow 0$  in order to obtain  $H_0$ , but rather we combine data in the range where they exist and estimate  $H_0$  from the consistency of distances. An extrapolation to  $z \rightarrow 0$  would be extremely sensitive to the choice of kernel and would not necessarily be a fair representation of the expansion rate in the redshift range where data do not exist [63,64].

In the past year, many valuable approaches to estimating  $H_0$  have been put forward; see, e.g., Refs. [5,6,65–70] for approaches that avoid calibration of the data while assuming a parametrization for the cosmological model. Of course, much work has focused on the calibration of the data with external information to obtain  $H_0$  with minimal dependence on the cosmological model (e.g., anchored SNe [2,4] and BAO [48,55,56,71]). With this work, we attempt to further reduce the assumptions. In addition, there is a subtle but important difference with previous approaches that used GP regression to reconstruct  $H(z)$  from expansion history data and extrapolated the outcome to redshift zero to obtain  $H_0$  [72–74]. We use Gaussian process techniques but only to interpolate distance data strictly within their redshift range, greatly reducing the kernel dependence of our results. Strong lensing time delay measurements also offer a way to measure  $H_0$  (see, e.g., Refs. [75,76]); however, the uncertainty on the final result is significantly enlarged (up to 10%) once one takes into account the uncertainties in the choice of the lens mass model [77].

### IV. RESULTS

Combining all seven reconstructed  $H_0$ , we derive a 2% constraint on the value of the Hubble speed,  $H_0 = 68.5 \pm 1.5$  km/s/Mpc. Our result is competitive with current measurements from [2,4,5,77,78] and robust to a revision of the systematics in CC measurements [79] as we discuss in Appendix B. Our value for  $H_0$  is in a  $2.5\sigma$  discrepancy with the value of SH0ES [2] and around  $1\sigma$  away from the Planck result. In the following we elaborate more on both of these aspects, as they crucially unveil important insights on the calibration of SNIa and on possible new physics.

From our value of  $H_0$ , we infer the SNIa absolute magnitude  $M_B = -19.355 \pm 0.054$ , in  $2.5\sigma$  tension with the calibrated magnitude of SH0ES, i.e.,  $M_B = -19.22 \pm 0.04$ . This discrepancy can be traced back to a constant systematic offset in the SNIa calibration of  $|\delta M| = 0.138 \pm 0.067$ , consistent with the results of [10,12,46]. Our result is in perfect agreement with the  $H_0$  measurement from TRGB [23,80] and suggests that the discrepancy with SH0ES may just be related to an unaccounted-for systematics in the SNIa calibration via Cepheids.

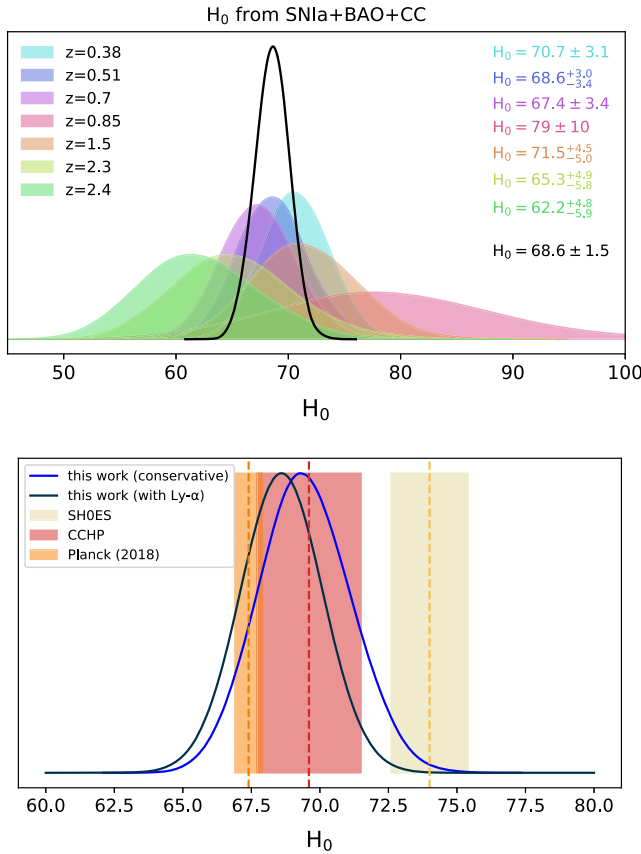


FIG. 3. Top panel: PDFs for the Hubble parameter obtained from Eq. (6), at the seven redshift points of BAO data (shaded curves). The solid black line represents the combined PDF (full result). Bottom panel: PDF for  $H_0$  corresponding to our full result (solid black curve) and conservative result (solid blue line), along with recent constraints from SH0ES [2], TRGB [23], and Planck [5]; shaded regions represent the  $1\sigma$  interval.

In obtaining our result for  $H_0$ , we use all the BAO data, even though the Lyman- $\alpha$  points fall outside the redshift range of CC and SNIa and are therefore more prone to kernel-dependent results. By looking at the means of the distributions in Fig. 3, it is clear that these two points give a very low mean value for  $H_0$ , and this effectively lowers the final, combined value. Their contribution to the total error is instead negligible. We check that the drop in the value of  $H_0$  is not a feature introduced by the kernel choice. Removing those two points, we obtain a slightly higher value of the Hubble constant with a similar precision, i.e.,  $H_0 = 69.5 \pm 1.7$  km/s/Mpc. We refer to this constraint as conservative, and hereafter we will quote it as our main result.

In combining our measurements via the DDR, we implicitly assume that the different data sets trace the underlying expansion history equally well. An offset in their ability to catch features in  $H(z)$  would show up as an apparent redshift dependence of  $H_0$ —in our case, as a discrepancy between full and conservative results. CC are direct measurements of the expansion history, while SNIa are sensitive to the integral of  $H(z)$  over the line of sight. Therefore, we expect a slight lag in their tracing of  $H(z)$ , which indeed can be noticed by comparing our reconstructions of the luminosity distance from SNIa to that of the angular diameter distance from BAO + CC (see Fig. 2). One clearly notices that the BAO + CC reconstruction starts showing a mild departure from  $\Lambda$ CDM at around  $z \sim 1$ , while the SNIa reconstruction shows hints of deviations only around  $z \sim 1.5$ . In our analysis this lag shows up as a drop in the binned values of  $H_0$  for higher redshifts, but it actually corresponds to a mild deviation of  $H(z)$  from  $\Lambda$ CDM, i.e.,  $X(z) \neq -1$  at high redshift. This falls well within the  $1\sigma$  confidence interval of the GP reconstruction; therefore, it does not constitute any evidence of a deviation but rather just a trend in line with the findings of [24,81–83]. Recently, some analyses of the Pantheon data set highlighted a possible transition of the SNIa magnitude at  $z \lesssim 0.2$  [84–86]. These trends are noticed in the low redshift tail, and their interpretation is possibly very different from the one of the higher redshift trend that we find. Finally, it is tantalizing to notice that our trend is of the same level of the shift between the late-time TRGB measurement of  $H_0$  and Planck’s, and in fact, it would bring the two values in even better agreement. Were upcoming measurements to corroborate a discrepancy between CMB and TRGB inferences of  $H_0$ , a physical trend in  $H(z)$  would resolve it.

## V. DISCUSSION AND CONCLUSIONS

In conclusion, we have introduced an approach to measuring the Hubble parameter which relies only on a few foundational assumptions at the basis of the distance duality relation and, importantly, uses a combination of geometrical data that do not need calibration nor the

assumption of a cosmological model. We use GP regression techniques to fit the data *uniquely* in the redshift range where they exist, avoiding possibly biasing extrapolation of  $H(z)$  to  $z = 0$ . Our result of  $H_0 = 69.5 \pm 1.7$  km/s/Mpc shows the possibility of measuring  $H_0$  at the percentage level with the least possible assumptions.

Whereas current data do not allow for a complete resolution of the Hubble tension, our method clearly shows that an adjustment in the calibration of the SNIa—i.e., setting  $M_B = -19.355 \pm 0.054$ ,  $2.5\sigma$  lower than SHOES calibration—brings local measurements in agreement. We also show that a mild dynamical feature in  $H(z)$  at intermediate redshift would further lower the latter, bringing them in even better agreement with the early-time measurement of Planck.

The data analysis technique that we presented is promising in terms of leading to competitive constraints that rely on the least possible theoretical assumptions. While we have focused on the Hubble parameter, it offers an interesting alternative to the popular Monte Carlo Markov chain (MCMC) technique, which has been pivotal for the estimation of cosmological parameters, by not requiring the choice of any cosmological model. This frees us from theoretical biases which can be particularly limiting when tackling tensions among data sets, and it allows a more direct inference of the underlying physics from data. An interesting example is an alternative way of estimating the sound horizon  $r_s$ , independently of the cosmological model. This can be achieved by combining SNIa distance measurements, marginalized over their absolute magnitude, with transverse BAO measurements, i.e.,  $D_A(z)/r_s$  (see [38–41] for previous work in this direction).

## ACKNOWLEDGMENTS

We thank Guadalupe Cañas Herrera, Alice Garoffolo, Archisman Ghosh, William Giarè, Wendy Freedman, Matteo Martinelli, Subodh Patil, and Adam Riess for helpful discussions. We acknowledge support from the NWO and the Dutch Ministry of Education, Culture and Science (OCW) (through NWO VIDI Grant No. 2019/ENW/00678104 and from the D-ITP consortium).

## APPENDIX A: GPMC METHOD

A Gaussian process is defined as “a collection of random variables, any finite number of which have a joint Gaussian distribution” [87]. A GP therefore generalizes a Gaussian probability distribution with the key difference that a probability distribution describes finite-dimensional random variables while a GP describes the properties of functions. This allows one to reconstruct an unknown function  $\phi(z)$  given the function values  $z$  in terms of the mean and covariance (also known as the kernel) of the GP. Without loss of generality, the GP mean can always be set to zero, and the GP is therefore specified only by its

covariance or kernel. Kernels are parametrized by a set of hyperparameters that, once specified, completely define the GP behavior and must be fitted to the data. The GP can be used to solve the ordinary least square problem in a Bayesian fashion, minimizing a likelihood marginalized over the unknown function  $\phi(z)$  [87]. This is typically called a GP regression. In this paper we used this procedure to reconstruct our SNIa and CCH data, but to fix the kernel hyperparameters we rely on the maximization of the following  $\chi^2$  likelihood:

$$-2 \ln \mathcal{L} = (\hat{\phi} - \phi)^T \Sigma^{-1} (\hat{\phi} - \phi). \quad (\text{A1})$$

The above likelihood contains the data covariance matrix  $\Sigma$  for  $\phi(z)$ , the data corresponding to a given observable. Here  $\hat{\phi}(z)$  is the GP reconstruction for the observable. This approach allows us to avoid kernel-dependent results, typical of the marginal likelihood method (see, e.g., Refs. [72,88]). For the Pantheon data we proceed by using the full data sets (1048 SNIa) for the GP reconstruction, while we compute the likelihood on the binned data set (30 binned SNIa). For the cosmic chronometers, we instead use the collection of Table I for the GP reconstruction, and we compute the likelihood on a set of six measurements of  $E(z)$  obtained by combining the Pantheon data set and the high redshift SNIa of the Multi-Cycle Treasury (MCT) program [89].

Our results are basically insensitive to the choice of the GP kernel in the range, i.e.,  $0.05 \lesssim z < 2$ , where the data are abundant with a shift between the reconstructed distance that is much smaller than the  $1\sigma$  uncertainty of the GP reconstruction. The reconstruction at  $z > 2$  may depend significantly on the kernel; however, we find that this concerns only the error of the reconstruction and that the

TABLE I. Collection of  $H(z)$  measurements from cosmic chronometers.

$z$	$H(z)$	Reference	$z$	$H(z)$	Reference
0.07	$69.0 \pm 19.6$	[32]	0.4783	$80.9 \pm 9.0$	[35]
0.09	$69.0 \pm 12.0$	[33]	0.48	$97.0 \pm 62.0$	[33]
0.12	$68.6 \pm 26.2$	[32]	0.593	$104.0 \pm 13.0$	[34]
0.17	$83.0 \pm 8.0$	[33]	0.68	$92.0 \pm 8.0$	[34]
0.179	$75.0 \pm 4.0$	[34]	0.781	$105.0 \pm 12.0$	[34]
0.199	$75.0 \pm 5.0$	[34]	0.875	$125.0 \pm 17.0$	[34]
0.2	$72.9 \pm 29.6$	[32]	0.88	$90.0 \pm 40.0$	[33]
0.27	$77.0 \pm 14.0$	[33]	0.9	$117.0 \pm 23.0$	[33]
0.28	$88.8 \pm 36.6$	[32]	1.037	$154.0 \pm 20.0$	[34]
0.352	$83.0 \pm 14.0$	[34]	1.3	$168.0 \pm 17.0$	[33]
0.3802	$83.0 \pm 13.5$	[35]	1.363	$160.0 \pm 33.6$	[36]
0.4	$95.0 \pm 17.0$	[33]	1.43	$177.0 \pm 18.0$	[33]
0.4004	$77.0 \pm 10.2$	[35]	1.53	$140.0 \pm 14.0$	[33]
0.4247	$87.1 \pm 11.2$	[35]	1.75	$202.0 \pm 40.0$	[33]
0.44497	$92.8 \pm 12.9$	[35]	1.965	$186.5 \pm 50.4$	[36]
0.47	$89.0 \pm 49.6$	[47]			

results obtained with different kernels are highly consistent with one another; see also Fig. 1. Therefore, we select the GP reconstruction associated with the kernel giving the lowest  $\chi^2$ . These are, respectively, a rational quadratic kernel for the CC data and a Matern kernel [87] with the parameter  $\nu = 5/2$  for the Pantheon data set [see also Eqs. (A2) and (A3)]. For completeness we report here the analytical form of the RatQ kernel [87],

$$\kappa(z_i, z_j)_{\text{RatQ}} = \sigma_M^2 \left( 1 + \frac{d(z_i, z_j)}{2\alpha\ell} \right)^{-\alpha}, \quad (\text{A2})$$

and the general form of the Matern kernel,

$$\kappa(z_i, z_j) = \sigma_M^2 \frac{\left( \frac{\sqrt{2\nu}}{\ell} d(z_i, z_j) \right)^\nu}{\Gamma(\nu) 2^{\nu-1}} K_\nu \left( \frac{\sqrt{2\nu}}{\ell} d(z_i, z_j) \right), \quad (\text{A3})$$

where  $K_\nu(\cdot)$  and  $\Gamma(\cdot)$  are the modified Bessel and Gamma functions while  $d(z_i, z_j)$  is the Euclidean distance between  $z_i$  and  $z_j$ .

Once the GP reconstruction is complete, we obtain a continuous set of PDFs representing  $\phi(z)$  at every  $z$ . This feature of the GP regression allows us to compute the values of  $H_0 d_L(z)$  (from SNe) and  $H(z)$  (from the CC) at the BAO redshifts. Specifically, we draw  $10^4$  realizations of the expansion rate  $H(z)$  from the GP fit to the CC data. We then combine these realizations with the unanchored BAO data  $H(z) d_A(z)$  to infer the angular diameter distance  $d_A(z)$ . Similarly, we draw  $10^4$  realizations of the unanchored SNIa distance  $H_0 d_L(z)$  from the GP fit to the SNIa data. Finally, we combine the two reconstructions by means of Eq. (6) in the main text to get an estimate of the PDF of  $H_0$  at each of the BAO redshifts.

As a final step, we multiply together all the PDFs of  $H_0$  into a single PDF from which one can easily extrapolate the mean and variance by employing an inverse transform sampling. In this way, we take into account the correlations between individual  $H_0$  and their errors, without making any specific assumption about the form of the PDFs (e.g., approximating them to Gaussian PDFs). In Appendix C we review the impact of using such a likelihood to combine the seven reconstructed  $H_0$  PDFs.

## APPENDIX B: SYSTEMATICS OF THE CC MEASUREMENTS

In our approach, SNIa and BAO data effectively constrain the evolution with redshift  $E(z)$ , while CC measurements set an absolute scale by providing the value of  $H(z)$  at each redshift. It is therefore important to thoroughly assess the systematics in the CC measurements that could affect our  $H_0$  inference. CC measurements build on the following relation between  $H(z)$  and the differential time-redshift relation:  $H(z) = \frac{-1}{1+z} \frac{\Delta z}{\Delta t}$ . While it is straightforward to measure  $\Delta z$  through spectroscopic observations,

TABLE II. BAO data used in this work given in terms of  $d_M = (1+z)d_A$  and  $d_H = cH(z)^{-1}$ .

Type	$z$	$d_M/r_s$	$d_H/r_s$	Reference
BOSS galaxy-galaxy	0.38	$10.27 \pm 0.15$	$24.89 \pm 0.58$	[48]
eBOSS galaxy-galaxy	0.51	$13.38 \pm 0.18$	$22.43 \pm 0.48$	[48]
	0.70	$17.65 \pm 0.30$	$19.78 \pm 0.46$	[49,50]
	0.85	$19.50 \pm 1.00$	$19.60 \pm 2.10$	[51,52]
	1.48	$30.21 \pm 0.79$	$13.23 \pm 0.47$	[53,54]
eBOSS Ly- $\alpha$ -Ly- $\alpha$	2.34	$37.41 \pm 1.86$	$8.86 \pm 0.29$	[55]
eBOSS Ly- $\alpha$ -quasar	2.35	$36.30 \pm 1.80$	$8.20 \pm 0.36$	[56]

measuring  $\Delta t$  is a more challenging quest, which requires standard clocks, typically provided by differential ages of passively evolving stellar populations.

The possible sources of error in CC data come from uncertainties in modeling this stellar population [35,36,79,90,91] and can be summarized as follows: The CC measurements require one to select an unbiased tracer of the evolution of the differential age of the universe with redshift, and it is important to assess the impact of a subdominant, young stellar population; passively evolving galaxies have been found to be an optimal tracer of the cosmic differential age, yet they cannot be exactly described as composed of a single stellar population, and one needs to assess the impact of assuming more realistic star formation history (SFH); the metallicity of the stellar population is often used as a prior in the calibration of the relative age of a stellar population, and thus the uncertainties in modeling the stellar population metallicity must be included in the total error budget; finally, the CC measurements employ a stellar population synthesis (SPS) model to calibrate the relative stellar age; the uncertainties coming from different modeling of the SPS are also a possible source of systematics.

The CC data that we use for our main analysis (see Table I) already include the uncertainties associated with the SFH and the stellar metallicity [35,36,90]. The contribution of residual stellar population was shown to be negligible for this data set [91]. Here, we further consider the inclusion of SPS model uncertainties following the results of [79], where the latter were shown to contribute an additional  $\lesssim 16\%$  uncertainty in the CC measurements of  $H(z)$ , in the worst-case scenario. To include this error we first reconstruct the evolution of the SPS error with redshift through a GP fit on the values reported in the third column of Table 3 in [79]. We then sum in quadrature the reconstructed error to that reported in Table I, and we repeat our procedure to derive an estimate of  $H_0$ . We find that the effect of adding the SPS uncertainty is rather small, increasing the error of our fit by only  $\sim 0.5$  km/s/Mpc (consistently with [70]) and leading to  $H_0 = 69.7 \pm 2.1$  km/s/Mpc in the conservative case and  $68.9 \pm 2.1$  km/s/Mpc when Ly- $\alpha$  BAO are also included in the fit. Our main conclusions therefore remain the same, with a  $2\sigma$  shift with SH0ES that can be explained by a

corresponding offset in the absolute magnitude, and a  $\sim 1\sigma$  shift with Planck that may relate to a mild dynamical feature in  $H(z)$ .

### APPENDIX C: LIKELIHOOD OF THE SEVEN $H_0$ PDFs

In combining the seven PDFs for  $H_0$  obtained via the DDR, we have relied on a likelihood obtained by multiplying the marginalized PDFs, i.e.,  $\mathcal{L} = \prod_{i=0}^7 P_i(H_0)$ . Since these PDFs are monodimensional, the prior range for  $H_0$  used to calculate the posterior of the final  $H_0$  is chosen to sample the tails of the posterior. Given the uncertainty of around 2 km/s/Mpc expected on our final  $H_0$  constraint, we choose this prior to be  $H_0 \in [60, 80]$ . Correspondingly, we divide the prior range in 1000 equispaced bins, and we calculate the probability given by each PDF in each bin; then, we multiply them together to get the value of the likelihood according to our previous definition.

The reason to use a likelihood constructed from the marginalized PDFs is to optimally take into account both the shape and the correlations of our  $H_0$  measurements without including additional assumptions in the pipeline. In particular, our measurements show significant non-Gaussian behavior, and we cannot employ a multivariate Gaussian likelihood without introducing a bias.

This is due to the fact that the multivariate, by construction, assumes that each measurement has to be Gaussian distributed, which is clearly not true in our case. However, it is important to note that if the PDF tends to be nearly Gaussian, then a multivariate would be the correct representation of the likelihood of our  $H_0$  measurements. In this case the PDF product will not be a good choice for the likelihood, as the marginalized distribution will not include any correlation. This consideration follows from the fact that the marginalized distributions of a multivariate are Gaussian PDFs and by taking into account that, without correlation, the multivariate reduces to a product of independent Gaussian distributions.

Therefore, it is important to assess the impact of correlation and non-Gaussianity on our final determination of  $H_0$ . This can be done by comparing the final results of the main text with that obtained from a multivariate



Gaussian fit where the mean and covariance of the measurements are algebraically calculated from the PDF samples of each  $H_0$  measurement. In particular, we define a chi-square likelihood of the form

$$-2 \ln \mathcal{L} = \sum_j (H_0 - \hat{H}_0^j)^T C_{jk}^{-1} (H_0 - \hat{H}_0^k), \quad (\text{C1})$$

where  $\hat{H}_0^j = \frac{1}{N} \sum_{i=1}^N H_0^{ji}$  is the sample mean and

$$C^{jk} = \frac{1}{N-1} \sum_{i=1}^N (H_0^{ij} - \hat{H}_0^j)(H_0^{ik} - \hat{H}_0^k) \quad (\text{C2})$$

the sample covariance.

Performing our analysis with this likelihood, we find that there are no differences in the error budget compared to the results obtained without the multivariate; i.e., it remains equal to 1.7 km/s/Mpc. However, we notice a shift in the mean of 0.5 km/s/Mpc towards a value higher than our main result. This effect persists unaltered with and without the inclusion of Ly- $\alpha$  BAO. In particular, we find that  $H_0 = 70 \pm 1.7$  km/s/Mpc Ly- $\alpha$  BAO are not included. This minimal shift can be traced back to the assumption of Gaussian PDFs that pushes the mean of each PDF to a slightly higher value than when this assumption is relaxed. However, this shift is negligible compared to the error budget of our conservative results; therefore, the multivariate Gaussian and PDF likelihood give consistent results.

- 
- [1] L. Verde, T. Treu, and A. Riess, *Nat. Astron.* **3**, 891 (2019).  
[2] A. G. Riess, S. Casertano, W. Yuan, L. M. Macri, and D. Scolnic, *Astrophys. J.* **876**, 85 (2019).  
[3] A. G. Riess *et al.*, *Astrophys. J. Lett.* **934**, L7 (2022).  
[4] A. G. Riess *et al.*, *Astrophys. J.* **826**, 56 (2016).  
[5] N. Aghanim *et al.* (Planck Collaboration), *Astron. Astrophys.* **641**, A6 (2020).  
[6] E. Di Valentino, A. Melchiorri, and J. Silk, *Phys. Lett. B* **761**, 242 (2016).  
[7] E. Calabrese, A. Slosar, A. Melchiorri, G. F. Smoot, and O. Zahn, *Phys. Rev. D* **77**, 123531 (2008).  
[8] E. Di Valentino, A. Melchiorri, and J. Silk, *Nat. Astron.* **4**, 196 (2019).  
[9] W. Handley, *Phys. Rev. D* **103**, L041301 (2021).  
[10] E. Mortsell, A. Goobar, J. Johansson, and S. Dhawan, *Astrophys. J.* **933**, 212 (2022).  
[11] E. Mortsell, A. Goobar, J. Johansson, and S. Dhawan, *Astrophys. J.* **935**, 58 (2022).  
[12] G. Efstathiou, arXiv:2007.10716.  
[13] R. I. Anderson, *Astron. Astrophys.* **658**, A148 (2022).  
[14] W. L. Freedman, *Astrophys. J.* **919**, 16 (2021).  
[15] E. Di Valentino, O. Mena, S. Pan, L. Visinelli, W. Yang, A. Melchiorri, D. F. Mota, A. G. Riess, and J. Silk, *Classical Quantum Gravity* **38**, 153001 (2021).  
[16] S. Vagnozzi, *Phys. Rev. D* **102**, 023518 (2020).  
[17] G. Efstathiou and S. Gratton, arXiv:1910.00483.  
[18] S. Aiola *et al.* (ACT Collaboration), *J. Cosmol. Astropart. Phys.* **12** (2020) 047.  
[19] S. K. Choi *et al.* (ACT Collaboration), *J. Cosmol. Astropart. Phys.* **12** (2020) 045.  
[20] D. Dutcher *et al.* (SPT-3G Collaboration), *Phys. Rev. D* **104**, 022003 (2021).  
[21] L. Balkenhol *et al.* (SPT-3G Collaboration), *Phys. Rev. D* **104**, 083509 (2021).  
[22] N. Khetan *et al.*, *Astron. Astrophys.* **647**, A72 (2021).  
[23] W. L. Freedman, B. F. Madore, T. Hoyt, I. S. Jang, R. Beaton, M. G. Lee, A. Monson, J. Neeley, and J. Rich, *Astrophys. J.* **891**, 57 (2020).  
[24] Y. Wang, L. Pogosian, G.-B. Zhao, and A. Zucca, *Astrophys. J. Lett.* **869**, L8 (2018).  
[25] I. M. H. Etherington, *Philos. Mag.* **15**, 761 (1933).  
[26] C. Zhou, J. Hu, M. Li, X. Zhang, and G. Fang, *Astrophys. J.* **909**, 118 (2021).  
[27] R. Holanda and W. da Silva, *J. Cosmol. Astropart. Phys.* **12** (2020) 027.  
[28] B. Xu and Q. Huang, *Eur. Phys. J. Plus* **135**, 447 (2020).  
[29] R. Holanda, V. Busti, and J. Alcaniz, *J. Cosmol. Astropart. Phys.* **02** (2016) 054.  
[30] R. Holanda, V. Busti, F. Lima, and J. Alcaniz, *J. Cosmol. Astropart. Phys.* **09** (2017) 039.  
[31] A. Rana, D. Jain, S. Mahajan, A. Mukherjee, and R. Holanda, *J. Cosmol. Astropart. Phys.* **07** (2017) 010.  
[32] C. Zhang, H. Zhang, S. Yuan, S. Liu, T.-J. Zhang, and Y.-C. Sun, *Res. Astron. Astrophys.* **14**, 1221–1233 (2014).  
[33] D. Stern, R. Jimenez, L. Verde, M. Kamionkowski, and S. A. Stanford, *J. Cosmol. Astropart. Phys.* **02** (2010) 008.  
[34] M. Moresco *et al.*, *J. Cosmol. Astropart. Phys.* **08** (2012) 006.  
[35] M. Moresco, L. Pozzetti, A. Cimatti, R. Jimenez, C. Maraston, L. Verde, D. Thomas, A. Citro, R. Tojeiro, and D. Wilkinson, *J. Cosmol. Astropart. Phys.* **05** (2016) 014.  
[36] M. Moresco, *Mon. Not. R. Astron. Soc.* **450**, L16 (2015).  
[37] D. Scolnic *et al.*, *Astrophys. J.* **859**, 101 (2018).  
[38] J. L. Bernal, L. Verde, and A. G. Riess, *J. Cosmol. Astropart. Phys.* **10** (2016) 019.  
[39] A. Heavens, R. Jimenez, and L. Verde, *Phys. Rev. Lett.* **113**, 241302 (2014).  
[40] L. Verde, J. L. Bernal, A. F. Heavens, and R. Jimenez, *Mon. Not. R. Astron. Soc.* **467**, 731 (2017).  
[41] L. Pogosian, G.-B. Zhao, and K. Jedamzik, *Astrophys. J. Lett.* **904**, L17 (2020).  
[42] D. Benndorf, J. F. Jesus, and S. H. Pereira, *Eur. Phys. J. C* **82**, 457 (2022).  
[43] E. Aubourg *et al.*, *Phys. Rev. D* **92**, 123516 (2015).  
[44] A. J. Cuesta, L. Verde, A. Riess, and R. Jimenez, *Mon. Not. R. Astron. Soc.* **448**, 3463 (2015).

- [45] S. Taubenberger, S. H. Suyu, E. Komatsu, I. Jee, S. Birrer, V. Bonvin, F. Courbin, C. E. Rusu, A. J. Shajib, and K. C. Wong, *Astron. Astrophys.* **628**, L7 (2019).
- [46] D. Camarena and V. Marra, *Mon. Not. R. Astron. Soc.* **495**, 2630 (2020).
- [47] A. Ratsimbazafy, S. Loubser, S. Crawford, C. Cress, B. Bassett, R. Nichol, and P. Väisänen, *Mon. Not. R. Astron. Soc.* **467**, 3239 (2017).
- [48] S. Alam *et al.* (BOSS Collaboration), *Mon. Not. R. Astron. Soc.* **470**, 2617 (2017).
- [49] J. E. Bautista *et al.*, *Mon. Not. R. Astron. Soc.* **500**, 736 (2020).
- [50] H. Gil-Marín *et al.*, *Mon. Not. R. Astron. Soc.* **498**, 2492 (2020).
- [51] A. Tamone *et al.*, *Mon. Not. R. Astron. Soc.* **499**, 5527 (2020).
- [52] A. de Mattia *et al.*, *Mon. Not. R. Astron. Soc.* **501**, 5616 (2020).
- [53] R. Neveux *et al.*, *Mon. Not. R. Astron. Soc.* **499**, 210 (2020).
- [54] J. Hou *et al.*, *Mon. Not. R. Astron. Soc.* **500**, 1201 (2020).
- [55] V. de Sainte Agathe *et al.*, *Astron. Astrophys.* **629**, A85 (2019).
- [56] M. Blomqvist *et al.*, *Astron. Astrophys.* **629**, A86 (2019).
- [57] N. Schöneberg, J. Lesgourgues, and D. C. Hooper, *J. Cosmol. Astropart. Phys.* **10** (2019) 029.
- [58] T. M. C. Abbott *et al.* (DES Collaboration), *Mon. Not. R. Astron. Soc.* **480**, 3879 (2018).
- [59] L. Salvati, L. Pagano, R. Consiglio, and A. Melchiorri, *J. Cosmol. Astropart. Phys.* **03** (2016) 055.
- [60] P. A. Zyla *et al.* (Particle Data Group), *Prog. Theor. Exp. Phys.* **2020**, 083C01 (2020).
- [61] L. Capparelli, E. Di Valentino, A. Melchiorri, and J. Chluba, *Phys. Rev. D* **97**, 063519 (2018).
- [62] F. Renzi, N. B. Hogg, M. Martinelli, and S. Nesseris, *Phys. Dark Universe* **32**, 100824 (2021).
- [63] G. Efstathiou, *Mon. Not. R. Astron. Soc.* **505**, 3866 (2021).
- [64] D. Camarena and V. Marra, *Mon. Not. R. Astron. Soc.* **504**, 5164 (2021).
- [65] K. Dutta, Ruchika, A. Roy, A. A. Sen, and M. Sheikh-Jabbari, *Gen. Relativ. Gravit.* **52**, 15 (2020).
- [66] C.-G. Park and B. Ratra, *Astrophys. Space Sci.* **364**, 134 (2019).
- [67] Y. Chen, S. Kumar, and B. Ratra, *Astrophys. J.* **835**, 86 (2017).
- [68] E. Di Valentino, A. Melchiorri, and O. Mena, *Phys. Rev. D* **96**, 043503 (2017).
- [69] E. Di Valentino, A. Mukherjee, and A. A. Sen, *Entropy* **23**, 404 (2021).
- [70] S. Vagnozzi, A. Loeb, and M. Moresco, *Astrophys. J.* **908**, 84 (2021).
- [71] S. Alam *et al.* (eBOSS Collaboration), *Phys. Rev. D* **103**, 083533 (2021).
- [72] A. Gómez-Valent and L. Amendola, *J. Cosmol. Astropart. Phys.* **04** (2018) 051.
- [73] A. Bonilla, S. Kumar, and R. C. Nunes, *Eur. Phys. J. C* **81**, 127 (2021).
- [74] H. Yu, B. Ratra, and F.-Y. Wang, *Astrophys. J.* **856**, 3 (2018).
- [75] K. C. Wong *et al.*, *Mon. Not. R. Astron. Soc.* **498**, 1420 (2020).
- [76] T. Collett, F. Montanari, and S. Räsänen, *Phys. Rev. Lett.* **123**, 231101 (2019).
- [77] S. Birrer *et al.*, *Astron. Astrophys.* **643**, A165 (2020).
- [78] D. Pesce *et al.*, *Astrophys. J. Lett.* **891**, L1 (2020).
- [79] M. Moresco, R. Jimenez, L. Verde, A. Cimatti, and L. Pozzetti, *Astrophys. J.* **898**, 82 (2020).
- [80] W. L. Freedman *et al.*, *Astrophys. J.* **882**, 34 (2019).
- [81] G.-B. Zhao *et al.*, *Nat. Astron.* **1**, 627 (2017).
- [82] G. Risaliti and E. Lusso, *Nat. Astron.* **3**, 272 (2019).
- [83] M. Raveri, *Phys. Rev. D* **101**, 083524 (2020).
- [84] M. G. Dainotti, B. De Simone, T. Schiavone, G. Montani, E. Rinaldi, and G. Lambiase, *Astrophys. J.* **912**, 150 (2021).
- [85] L. Kazantzidis, H. Koo, S. Nesseris, L. Perivolaropoulos, and A. Shafieloo, *Mon. Not. R. Astron. Soc.* **501**, 3421 (2020).
- [86] E. Di Valentino, E. V. Linder, and A. Melchiorri, *Phys. Dark Universe* **30**, 100733 (2020).
- [87] C. E. Rasmussen and C. K. I. Williams, *Gaussian Processes for Machine Learning* (The MIT Press, Cambridge, MA, 2005).
- [88] S. Pandey, M. Raveri, and B. Jain, *Phys. Rev. D* **102**, 023505 (2020).
- [89] A. G. Riess *et al.*, *Astrophys. J.* **853**, 126 (2018).
- [90] M. Moresco, L. Verde, L. Pozzetti, R. Jimenez, and A. Cimatti, *J. Cosmol. Astropart. Phys.* **07** (2012) 053.
- [91] M. Moresco, R. Jimenez, L. Verde, L. Pozzetti, A. Cimatti, and A. Citro, *Astrophys. J.* **868**, 84 (2018).